A&A manuscript no.
(will be inserted by hand later)

Your thesaurus codes are:

ASTRONOMY
AND
ASTROPHYSICS
1.2.2008

An Interferometric Study of the Blue Compact Dwarf Galaxy IZW18 ⋆

A. R. Petrosian[1], J. Boulesteix[2], G. Comte[2], D. Kunth[3], and E. LeCoarer[4]

[1] Byurakan Astrophysical Observatory, Armenia
[2] Observatoire de Marseille, 2 Place le Verrier, F-13248 Marseille Cedex 04, France
[3] Institut d'Astrophysique de Paris, 98bis. Boulevard Arago, 75014, Paris, France
[4] Observatoire de Grenoble, Universite Joseph Fourier, 414, rue de la Piscine, Boite Postale 53X, F-38041, Grenoble Cedex, France

Received .....1996; accepted 1996

Abstract. We present high spatial resolution observations of the blue compact dwarf galaxy IZW18 performed in the Hα line with a scanning Fabry-Perot interferometer at the CFH telescope. Morphological structure of the galaxy in Hα and in the red continuum is investigated. We also analyse the velocity field of the ionized gas. Besides the two compact HII components of the main body we find a population of small HII regions in its surroundings whose diameter distribution and Hα luminosity function are consistent with those observed in dwarf irregular galaxies. In the main body of the galaxy besides of the NW and SE red continuum peaks which are displaced with respect to the Hα maxima, three new red condensations have been discovered. They have no clear Hα counterparts. The velocity field in IZW18 shows peculiar motions superimposed on a quite regular background implying solid-body rotation with a gradient of about 70 km s^{-1} kpc^{-1}. The Hα line profiles exhibit an asymmetric structure, except for the NW main compact component. At least part of this asymmetry could result from accreted and/or expelled surrounding gas from the main star-forming core(s) of the galaxy. Contrary to previous suggestions that the south-west and north-east extensions of this galaxy are diffused emission produced by bipolar emitting gas we provide evidence that they are HII regions powered by star formation sites. The redshift of the Zwicky's "flare" has been measured for the first time and corresponds to the same velocity as IZW18. In such a context the optical ridge that appears to be an isolated morphological structure has a shape that may result from the gravitational interaction with the Zwicky's "flare" if this latter is a neighbour extreme dwarf object.

Key words: galaxies-compact-individual(IZW18)-structure-ISM-kinematics and dynamics-star formation

1. Introduction

Extensive studies of Blue Compact Dwarf Galaxies (BCDGs) have revealed that a large fraction of them are chemically unevolved small systems undergoing violent star formation activity (Thuan 1987). The triggering mechanism of starbursts in BCDGs is still completely unknown. One of the approaches for understanding this mechanism is to investigate the morphological, kinematical and dynamical relationship between star–forming regions and their surrounding gas and also to search for global correlations between star–forming regions and the gas in various places of a galaxy. Since BCDGs are among the best candidates for genuine zero-redshift young galaxies their kinematical and dynamical state may give also some clues on the nature of dark matter (Tremaine & Gunn 1979).

The neutral gas component of some BCDGs has been kinematically studied with radio interferometers (Viallefond & Thuan 1983; Viallefond et al. 1987; Taylor et al. 1991). In the few objects studied so far, this gas shows core-halo distribution and some chaotic velocity superimposed on a regular velocity field indicative of a solid body rotation.

On the other hand the ionized gas component in BCDGs has a clumpy distribution and is mainly concentrated in at least one compact star–forming HII region immersed in an amorphous extended envelope of low luminosity ionized material (Kunth et al. 1988). The inner dynamics of HII regions in BCDGs has been investigated by Gallagher & Hunter (1983) and Lequeux et al. (1995).

Send offprint requests to: D. Kunth

⋆ Based on observations performed with the Canada-France-Hawaii Telescope

Velocity fields in BCDGs have been mapped using multi-slit observations (Tomita et al. 1993) and Hα Fabry-Perot interferometric observations (Thuan et al. 1987).

The combination of a Fabry-Perot interferometer with a large telescope provides high spatial and velocity resolution and allows to probe small scales in dwarf compact galaxies, yielding information on components not resolved on HI maps (Thuan et al. 1987). Further, a BCDG not only has a small angular size and a compact distribution but at the same time exhibits very strong and narrow emission lines. For this reason BCDGs are ideal targets for Fabry-Perot interferometer observations. In this paper we present results relevant to the extreme metal–poor BCDG IZW18 (Mrk116).

IZW18 first was described by Zwicky (1966) as a "double system of compact galaxies". Later IZW18 became an outstanding extragalactic object when Sargent & Searle (1970) characterized it as "isolated extragalactic HII region" and found that it is extremely metal poor as compared to the Sun (Searle & Sargent 1972). Later on after 25 years more than 100 scientific papers have been addressed to this galaxy. But among them, articles which contain data on IZW18 as a extended two component system (Petrosian et al. 1978; Mazzarella & Boroson 1993) are rare. Optical imagery of IZW18 has been published by Hua et al. (1987), Davidson et al. (1989, hereafter DKF89), Dufour & Hester (1990, hereafter DH90) and Martin (1996, hereafter M96). Broadband WFPC2 on HST observations were carried out by Hunter & Thronson (1995, hereafter HT95). GHRS HST spectroscopic observations revealed very low oxygen abundance in the HI envelope of this galaxy (Kunth et al. 1994, but see Pettini & Lipman 1995 for a critical comment of this result). HI line interferometric observations by Lequeux & Viallefond (1980), Viallefond et al. (1987) and radio continuum observations by Klein et al. (1983) were also reported. Probably due to its very low metal-content IZW18 has been detected neither by IRAS (Kunth & Sevre 1986; Mazzarella et al. 1991) nor in CO millimeter line (Arnault et al. 1988).

As part of our high spatial and spectral resolution study of genuine BCDGs, in this paper we present the Hα scanning Fabry-Perot interferometric observations of IZW18. We describe the observations and data reduction in Section 2. Results are presented in Section 3 and are discussed in Section 4. We summarize our conclusions in Section 5. We shall adopt 10 Mpc as the distance to IZW18, based on a recessional velocity of 763 km s^{-1} and a Hubble constant H_o = 75 km s^{-1} Mpc^{-1}. The linear scale is therefore 48 pc arcsec^{-1}.

2. Observations and data reduction

Observations have been performed at the Cassegrain focus of the 3.6 m Canada-France-Hawaii telescope on November 22 1986, with the CIGALE instrument (Boulesteix et al. 1983). It consists of a focal reducer (f/8 - f/2), and a piezo-electrically scanned Fabry - Perot interferometer from Queensgate Instruments interfaced with a two dimensional photon counting camera. The optical setup of the f/2 focal reducer allows a field of view of 6.′2 x 6.′2. The original photon addresses are computed on a 512 x 512 pixel grid on the detector, giving a scale of 0.″725 per pixel.

The Fabry-Perot etalon operates with an interference order of 798 at the rest wavelength of Hα providing a free velocity range of 375 km s^{-1}. The corresponding free spectral range was scanned through 21 scanning steps (each step corresponding to a given spacing of the plates of the interferometer), the 21th step being equivalent to the 1st one. Thus the velocity sampling step is 18.8 km s^{-1} . Each scanning step has been exposed 18 x 10s. The total exposure time was 60 minutes (18x10x20s). A neon lamp emitting the 6598.9 Å line was used for wavelength calibration.

The final product of the 20 elementary interferograms processing is a 3 - dimensional data cube with 2 spatial and one velocity coordinates. For each pixel with reasonably high S/N ratio the radial velocity, the Hα line profiles and the Hα and continuum fluxes are derived from this cube.

The night sky OH emission line at 6577.2 Å has a wavelength value close to that of the redshifted IZW18 Hα emission. An interactive routine was used to subtract the night sky line. The radial velocity at each pixel was then extracted by a barycentric technique (Laval et al. 1987). The barycenter of the Hα line is found with an accuracy much better than the interferometer scanning–step (18.8 km s^{-1}).

From the data cube, Hα line profiles are built for each pixel. Gaussian curves were fitted to the observed profiles to investigate their structure and derive velocity dispersions due to macroscopic gas motions. The velocity dispersion of the Gaussian profile which best fits the observed profile is defined by

$$\beta^2 = \beta_{\rm obs}^2 - \beta_{\rm i}^2 - \beta_{\rm th}^2$$

where $\beta_{\rm th}$ is the thermal broadening function and $\beta_{\rm i}$ the instrumental profile. According to the value T_e = 18000 K of the nebular gas electron temperature of IZW18 (Dufour et al. 1988) the thermal broadening $\beta_{\rm th}$ is estimated as 12.2 km s^{-1} (Dopita 1972). The instrumental profile determined by scanning the neon 6598.95 Å line, was found to be well fitted by a Gaussian with velocity width $\beta_{\rm i}$ = 14.4 km s^{-1}. The observed profile is described with $\beta_{\rm obs}$ = 0.425 FWHM.

The total intensity profile for each pixel when adding up the 21 channels, contains information about the monochromatic emission as well as the continuum emission of the object. CIGALE observations enable us to separate monochromatic emission from continuum emission (see details in Laval et al. 1987). It is thus possible to restore pure monochromatic Hα images of IZW18, completely free from the underlying stellar continuum. The

continuum subtracted Hα line images of IZW18 were calibrated using the absolute flux published by Davidson & Kinman (1985) and DH90. In the same way a continuum map free from Hα line contribution was built. The FWHM of the interference filter was 10 Å which determined the bandwidth of the image continuum of IZW18. Continuum flux calibrations were based on the assumption that the continuum slope of IZW18 is given by

$$f(\lambda) = A\lambda^{-2.5}$$

(Davidson & Kinman 1985) and on absolute flux values at 6600 Å given by DKF89. In making a continuum model we have neglected the underlying stellar abosrption since according to Skillman and Kennicutt (1993) the absorption component in Hα is of the order of 2Å while the Hα emission has an equivalent width more than two order of magnitude larger (465Å). For the confirmation of faint detected emission–line features such as small narrow-line HII regions, a careful check was made on the series of channel maps: a feature has been considered as certain ONLY if seen on at least two consecutive channel maps.

Hα and continuum luminosities are derived from the measured fluxes and are corrected for extinction using values adopted by Dufour et al. (1988).

Since the image of IZW18 is sufficiently small to be located in the central part of the field of view where all the causes for sensitivity variations are reduced (optical system, filter combination, detector inhomogeneities) the original images of the galaxy were not flat-fielded.

3. Results

When the interferometer is scanning the object, the monochromatic emission of this latter is modulated by the interference pattern while the continuum emission remains unaffected. This enables to distinguish line and continuum emission with a much higher contrast than with simple images obtained through interference filters.

Figures 1 and 2 show the logarithmic contour maps of respectively the red continuum emission and the monochromatic Hα emission in absolute flux units across the main body of IZW18. The selectivity of the Fabry-Pérot interferometer due to its high finesse (F=16 measured on calibration frames) allows a very clear separation of the line and the continuum emissions. Furthermore, the overall system (FP + focal reducer) benefits from a very low level of scattered light, much below a percent, which ensures that the continuum map is free from additional line emission.

3.1. Quantitative red continuum morphology

In red continuum (Fig.1) the morphological structure of IZW18 is complex and new details appear which were not detected by DKF89. Some of these details have their counterparts on the HST WFPC2 frames (HT95). In the main body of the galaxy besides two known NW and SE red continuum components (DKF89) a third one (a) is observed half way between them close from the north of the HII region number 6 in HT95. We identify two other condensations: (b) to the north and (c) to the north-west of the NW compact red component. Among all the components NW dominates in size, surface and absolute brightness. Table 1 lists $\Delta\alpha$, $\Delta\delta$ positions of the photometric center of the components in arcsec with respect to the NW component. Positive values of $\Delta\alpha$ are to the east and positive $\Delta\delta$ to the north, effective diameters D in parsecs, surface brightness SB in units of 10^{-17}ergs cm^{-2} s^{-1} A^{-1} arcsec^{-2} and red magnitudes at 6600 Å. Table 1 also lists the same parameters for the Zwicky's "flare" (Zwicky 1966) - noted as the C satellite by DKF89 and DH90.

The comparison between the structure of the NW red component and its surroundings with that of HT95 frames shows that this component is coeval to an isolated HII region south to the main NW star-forming complex (HT95). A sharp cut-off in the NW red continuum brightness distribution is observed towards the (a) and SE components while it fades smoothly in the opposite direction towards the (b) component. The (b) component itself is located in the northern part of NW star–forming complex of HT95. At faint levels of brightness a west side "ledge" is observed. The (c) component is embedded into this ledge and has no direct counterpart on HST frames (HT95).

Besides the main body of the galaxy its outer envelope is also radiating in the red continuum. This radiation is not homogenous. It shows a clumpy structure extending to the NE direction up to a distance of about 740 pc from the NW component. Its patterns are located within the same region of the NE Hα shell of M96. Towards the SW the red continuum radiation extends in more homogeneous way by curving at its end to the west and its patterns closely follow the Hα arc–like structure DH90.

Stellar light as well as some nebular continuum contribute to the red continuum radiation of the outer envelope of the galaxy and its arc-like structure. To determine their respective contribution we have measured the L(Hα)/L(6600Å) ratios across these regions and compared the obtained values with model calculations provided to us by Mas-Hesse (private communication). Models show that the underlying nebular continuum should be less than 1 percent of our measured luminosity at 6600 Å .

3.2. Quantitative Hα morphology

Our Hα monochromatic image (Fig.2) completely reproduces the structural features which were identified in earlier observations (Hua et al. 1987; DKF89; DH90; HT95; M96; Ostlin et al. 1996). Let us underline some details.

We hereafter shall define an autonomous HII feature as the region which is inside its outermost closed contour. Both NW and SE condensations are isolated from

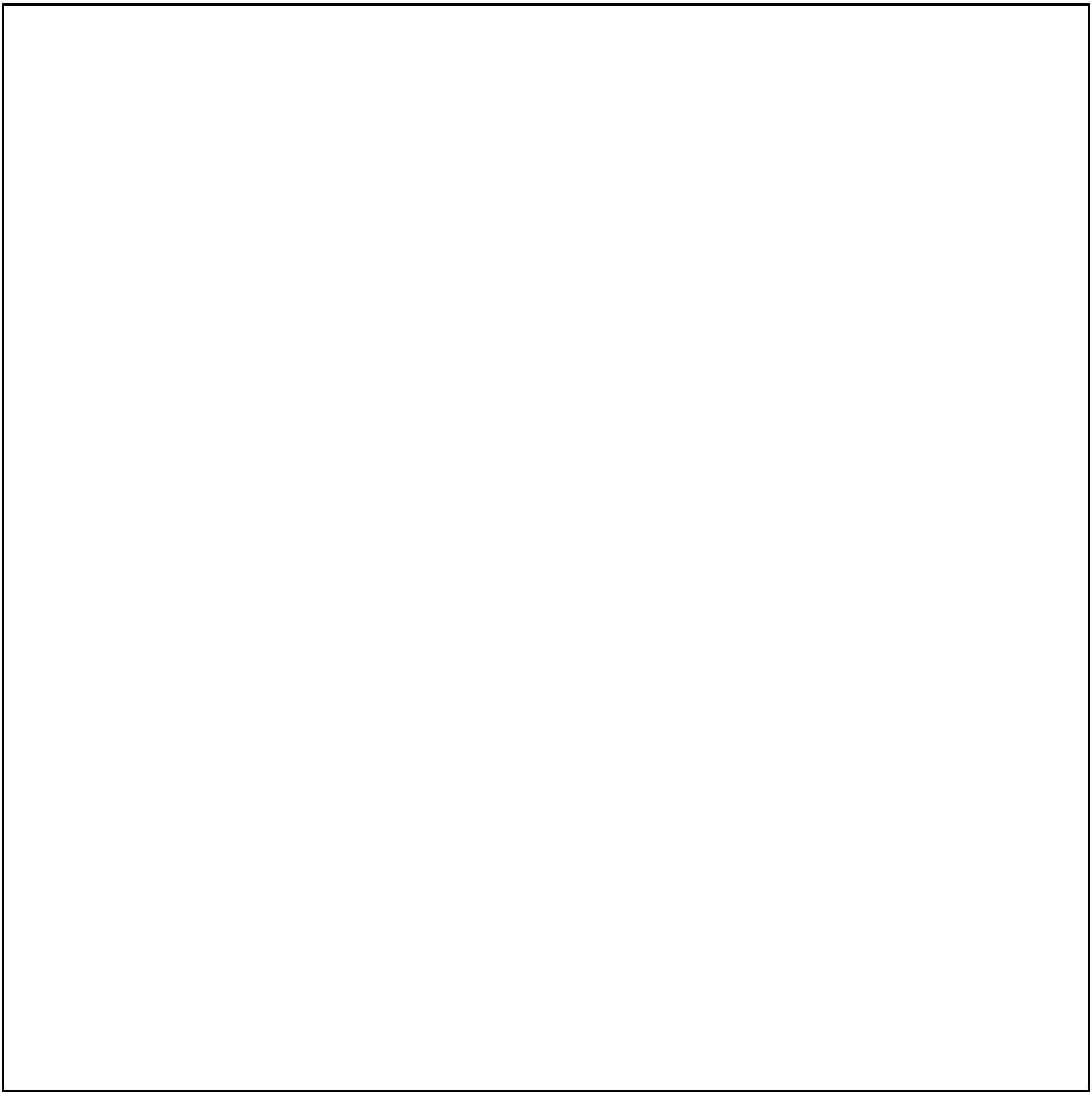

Fig. 1. The 6600Å red continuum map of IZW18. The lowest contour corresponds to a flux of $1.2 10^{-18}$ergs cm^{-2} s^{-1} A^{-1} per pixel. Contours are logarithmically spaced by a factor of 0.1. The insert is the detail view to central part of the galaxy. All morphological details are labelled.

the main body of the galaxy by an isophote corresponding to 4.5 10^{-15} ergs cm^{-2} s^{-1} arcsec^{-2} of surface brightness.

The NW component of IZW18 has a size of 195 x 117 pc^2, while the SE component is 157 x 117 pc^2. Note that the elongation of both components coincides with the elongation of the main body of the galaxy.

After correction from Galactic reddening the integrated Hα flux of NW and SE components come to be 1.3 10^{-13} ergs cm^{-2} s^{-1} and 6.3 10^{-14} ergs cm^{-2} s^{-1} respectively. At D = 10 Mpc these values correspond to Hα luminosities of 1.6 10^{39}ergs s^{-1} and 7.6 10^{38}ergs s^{-1}. Assuming Case B conditions and T_e = 18000 K (Dufour et al. 1988) these luminosities require conversion of 2.2 10^{51}

Table 1. Parameters for red continuum components

Component	$\Delta\alpha$ $''$	$\Delta\delta$ $''$	D pc	$SB(6600\AA)$ $10^{-17}\ ergs\ cm^{-2}\ s^{-1}\ A^{-1}\ arcsec^{-2}$	$m(6600\AA)$
NW	0	0	112	4.8	17.2
SE	2.9	-3.6	79	3.1	18.7
a	1.5	-1.5	56	3.2	19.2
b	-0.7	2.9	56	2.8	19.1
c	-2.9	1.5	40	4.0	20.2
C	-18.9	16.7	177	0.3	20.6

and 1.1 10^{51} ionizing photons s^{-1} requiring 47 and 23 O5V stars, assuming that an O5V star emits 4.7 10^{49} photons s^{-1} (Osterbrock 1989).

Star formation rates (from 0.1 to $100M_{\odot}$) in the NW and SE component are equal respectively to 4.7 $10^{-7}M_{\odot}\mathrm{yr}^{-1}$ pc^{-2} and 2.9 $10^{-7}M_{\odot}\mathrm{yr}^{-1}$ pc^{-2} assuming a Salpeter initial mass function (Hunter & Gallagher 1986).

Masses for the ionized gas in the NW and SE components have been estimated to be M(HII) = 7.3 $10^5M_{\odot}$ for the NW condensation and M(HII) = 3.4 $10^5M_{\odot}$ for the SE one, but these standard estimates are only indicative since these HII regions are far from being homogeneous as seen from the HST images.

The analysis of the mean spatial profiles of both components along the direction of their elongation and perpendicular to it, shows that the surface brightness peak of the NW Hα component is about 7.0 10^{-15}ergs cm^{-2} s^{-1} arcsec^{-2}, as compared to 6.4 10^{-15}ergs cm^{-2} s^{-1} arcsec^{-2} for the SE component. The Hα surface brightness gradient on the NW component across two perpendicular directions is different. It is gently sloping across the major axis of the component and much steeper in the perpendicular direction where according to HT95 a gap in ionized gas distribution is observed. The smoothest gradient is observed along the tail extending to the NW and wraps around to the west of the component. This feature was noted by DKF89, DH90 and also traced in the Hα maps of Hua et al. (1987). It is very well seen in Fig.1b of M96 and shows its detailed structure in Fig. 3 of HT95. As regards to the SE compact component, its Hα line brightness distribution is more homogeneous.

An interesting Hα feature is seen as a prominent winding ridge (DH90; HT95; M96; Ostlin et al. 1996) which expands south from the SE HII compact component, bends around to the NW , then turns back to the NE, making an half wrapping around the NW HII compact component. In the NW direction from the north-western boundary of the ridge about the same distance as from the NW component lies Zwicky's "flare" (Zwicky 1966). The ridge as an isolated structure is well shaped and has a conspicuous clumpy structure (HT95). As mentioned above (Sec.3.1) several patterns of the ridge radiate some red continuum. The continuum patterns do not follow the Hα clumps distribution. To understand the nature of the ridge we carefully tested the possibility of its link to the SE compact component. We conclude that there is not direct connection between them. From this point of view the ridge can be an isolated feature in the system. As it is noted by Viallefond et al. (1987) the two major star–forming areas in the main body of IZW18 are offset to the east of the double-lobed HI emission peak. The ridge wraps around the HI distribution peak opposite to the side where the main body of the galaxy is located, roughly following the steep contours marking the edge of the HI concentration.

Figure 3 shows the Hα image of the galaxy with the 6600 Å red continuum contours overlaid. One sees that the centroid of the NW Hα emission is located in the plateau, between the NW and (b) red continuum peaks and is displaced to the north of at $1''.5$ (72pc) from NW red continuum peak. As it was mentioned above (Sec. 3.1) the NW red component lies on an isolated stellar cluster-HII region complex (HT95). The (b) red peak is located on the NW Hα emission region and its connection with this star–forming region is more evident. The centroid of the SE compact Hα component is displaced by $1''.0$ (48pc) to the west of the SE red continuum centroid. This displacement between the continuum and Hα images is also evident from Fig.17 of HT95.

The Hα emission extends towards the NE and SW directions from the main body of IZW18 up to distance of about 1.2 kpc. The same order of extension is detected by DH90 and M96. As we stress in Sec.3.1 in the same direction but for smaller distances the clumpy red continuum emission was detected. The extended envelope detected in Hα line is not simply diffuse and shows numerous condensations (DH90).

We suggest that the isolated condensations that have been identified in the extended envelope of IZW18 as well as in the ridge are bonafide HII regions. This suggestion is supported by:

- the presence of clumpy red continuum radiation of stellar origin in the same fields where HII regions were identified.

- the detection of individual stars in the vicinity of the HII regions fields (Table 2 of HT95).

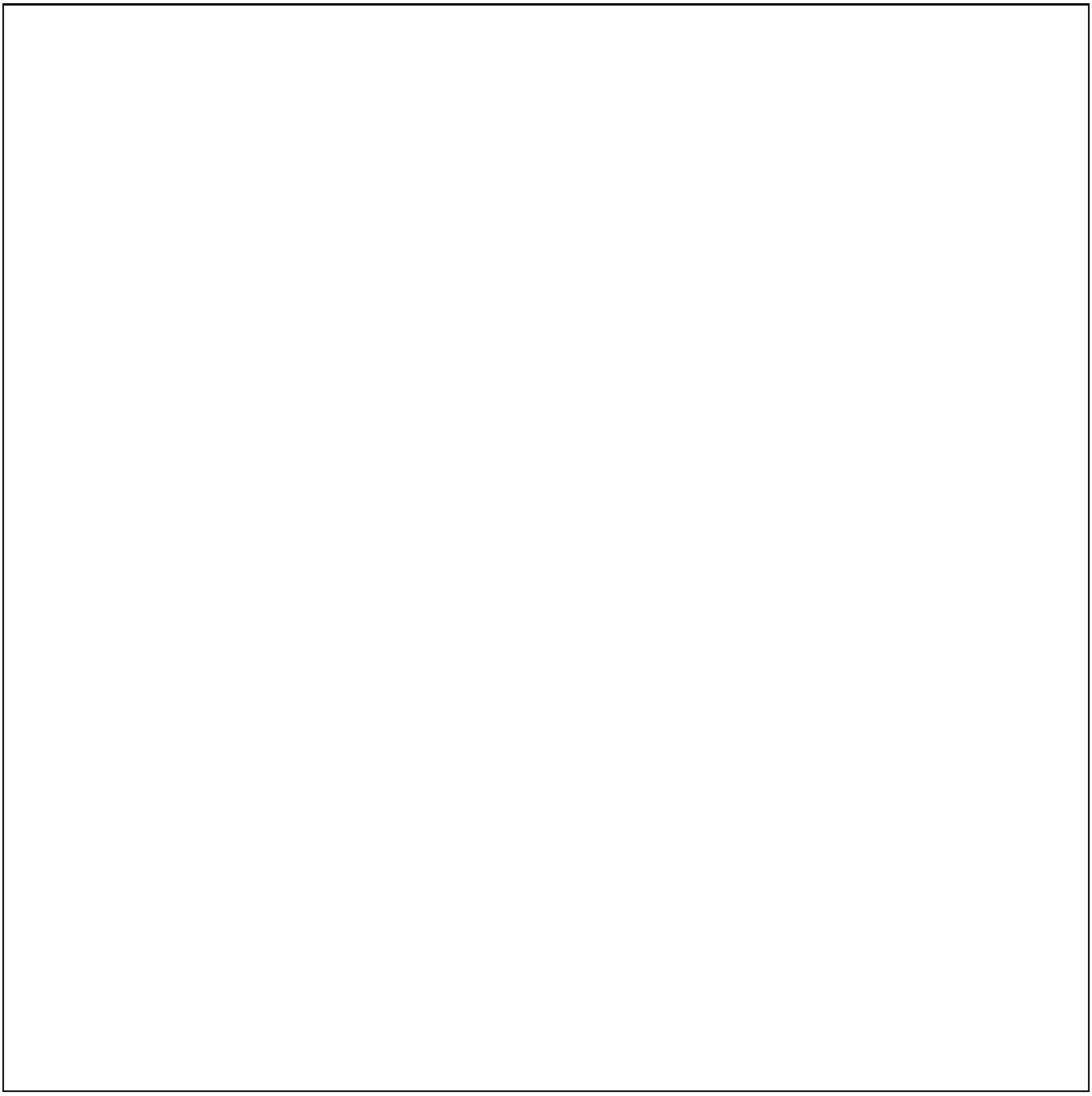

Fig. 2. Hα intensity map of IZW18. The lowest contour corresponds to a flux of a 10^{-17} $ergs$ cm^{-2}s^{-1} per pixel. Contours are logarithmically spaced by a factor of 0.2. HII regions and Zwicky's "flare" are labelled.

- the existence of nearly 15 well isolated HII regions in the main body of the galaxy also reported by HT95.

Since the Hα luminosity of any individual condensation is low (see below) the spectral type of the ionizing stars cannot be much earlier that B0 (Osterbrock 1989). At the distance of IZW18 such a star has a U magnitude equal to 25.4 which is roughly the limiting magnitude for the F336W frame of HT95. Nevertheless we carefully examined the positions of each individual HII regions to find such stars using the F336W frames of the HST–WFPC2 kindly given to us by Deidre Hunter. No such stars were found.

A total of 39 HII regions were identified. They have been detected on the total Hα map and their presence on at least two consecutive channel maps has been carefully checked. A majority of them are well seen on Fig.1 and

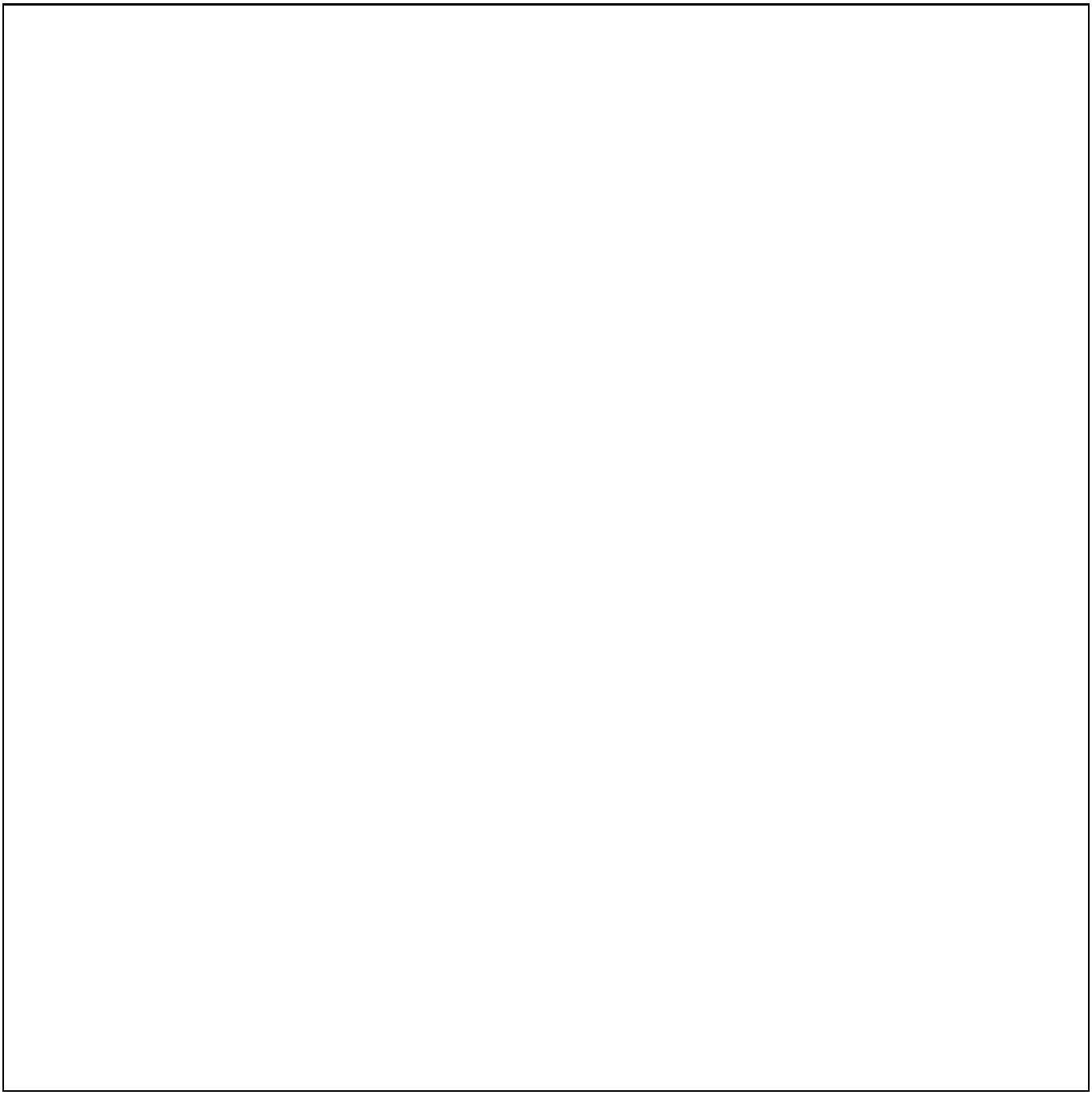

Fig. 3. Hα map of the IZW18 with 6600Å red continuum contours overlaid.

2 of Ostlin et al. (1996) and also on Fig. 1 of HT95. Observed HII regions are shown in the identification chart (Fig. 2) and listed in Table 2 which gives the following informations:

Column 1 lists the reference number given to individual HII regions as shown in the chart.

Columns 2 and 3 give the X,Y positions of the photometric center of the regions, in units of arcsec. The coordinate center is the Hα brightness peak in the NW component of the galaxy, positive values of $\Delta\alpha$ and $\Delta\delta$ are to the east and north respectively. The faintest Hα fluxes correspond to a S/N threshold of 5.

Columns 4 and 5 give the effective diameter D of the regions in arcsec and parsecs. An equivalent diameter was defined in terms of the limiting isophotal area A, of each HII region, according to the definition

$$D = 2(A/\pi)^{1/2}$$

Table 2. HII regions in IZW18

#	$\Delta\alpha$ $''$	$\Delta\delta$ $''$	D pc	$F(H\alpha)$ 10^{-16} $ergs\ cm^{-2}s^{-1}$	$L(H\alpha)$ 10^{36} $ergs\ s^{-1}$
1	10.9	-2.2	56	0.65	0.78
2	10.2	0.0	97	1.75	2.11
3	10.2	4.4	97	6.57	7.89
4	8.7	0.7	40	0.77	0.92
5	6.5	15.2	56	1.68	2.01
6	4.4	-10.9	56	0.54	0.64
7	3.6	-11.6	40	0.65	0.78
8	3.6	5.1	56	6.27	7.52
9	3.6	13.1	97	2.67	3.21
10	2.9	18.9	69	2.71	3.25
11	2.2	6.5	40	3.48	4.17
12	2.2	20.3	56	2.37	2.84
13	1.5	-16.7	97	4.55	5.46
14	1.5	18.9	40	1.68	2.01
15	0.7	-13.8	40	1.49	1.79
16	0.0	-8.7	40	6.69	8.03
17	0.0	15.2	56	2.06	2.47
18	-0.7	-14.5	79	3.97	4.77
19	-0.7	-10.9	69	7.03	8.44
20	-1.5	10.9	112	7.19	8.62
21	-1.5	13.1	69	1.75	2.11
22	-2.2	-17.4	56	2.79	3.35
23	-2.9	-13.8	97	9.48	11.30
24	88.0	-7.3	56	6.80	8.17
25	-5.8	-15.2	40	0.92	1.10
26	-6.5	-4.4	56	7.15	8.58
27	-7.3	3.6	40	3.02	3.62
28	-8.0	4.4	56	3.86	4.63
29	-9.4	-5.1	97	17.00	20.40
30	-10.2	-4.4	112	19.20	23.00
31	-10.9	1.5	56	1.64	1.97
32	-12.3	-1.5	40	1.91	2.29
33	-13.1	0.0	79	7.53	9.04
34	-14.5	4.4	97	5.58	6.70
35	-14.5	-2.2	56	6.92	8.30
36	-16.0	-13.1	97	5.73	6.88
37	-18.1	-8.7	56	1.30	1.56
38(C)	-21.1	17.0	63	0.77	0.92
39	-19.6	-13.1	40	0.80	0.96

The limits of each region are defined by the contour where the intensity of the Hα emission falls down to the average local intensity of the diffuse background.

Columns 6 and 7 list the total dereddened Hα fluxes of the regions in units of 10^{-16}ergs cm^{-2} s^{-1} and their Hα luminosities in units of 10^{36}ergs s^{-1}.

The faintest features listed in Table 2 have an Hα flux corresponding to a minimum number of photons that gives a signal-to-noise of 5. On Fig. 2 is marked and listed in Table 2 the Zwicky's "flare" (Zwicky 1966), component C by DH90. About 1.5 arcsec displacement exists between its red (Table 1) and Hα (Table 2) peaks. This displacement also appears on Fig. 2 of Ostlin et al. (1996).

3.3. HII regions size distribution and luminosity function

In Fig. 4 we show the cumulative diameter distribution built according to Table 2. It is consistent with an exponential law $N = N_0 \exp(D/D_0)$ where $D_0 = 24$ pc. This value is comparable with D_0 values found for the Irregular galaxies (Hodge 1983; Hodge et al. 1989; Hodge & Lee 1990).

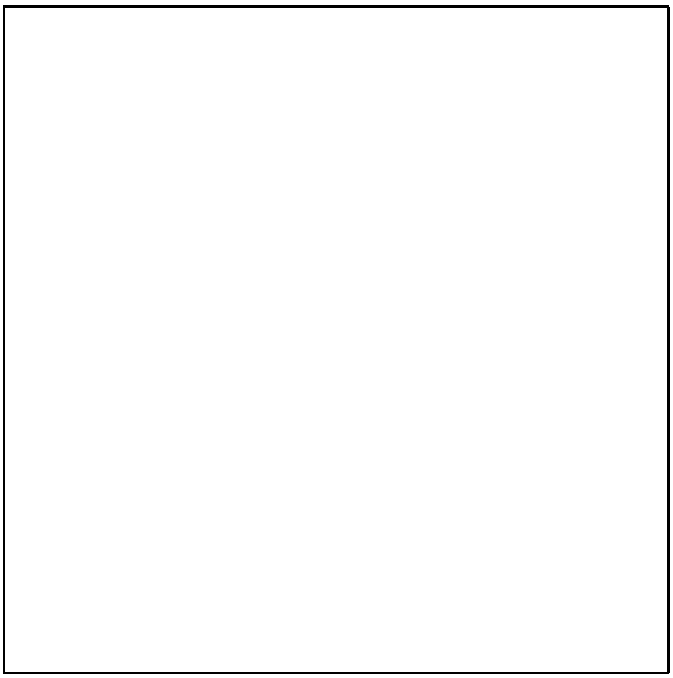

Fig. 4. Cumulative effective diameter distribution for the outer HII regions of IZW18.

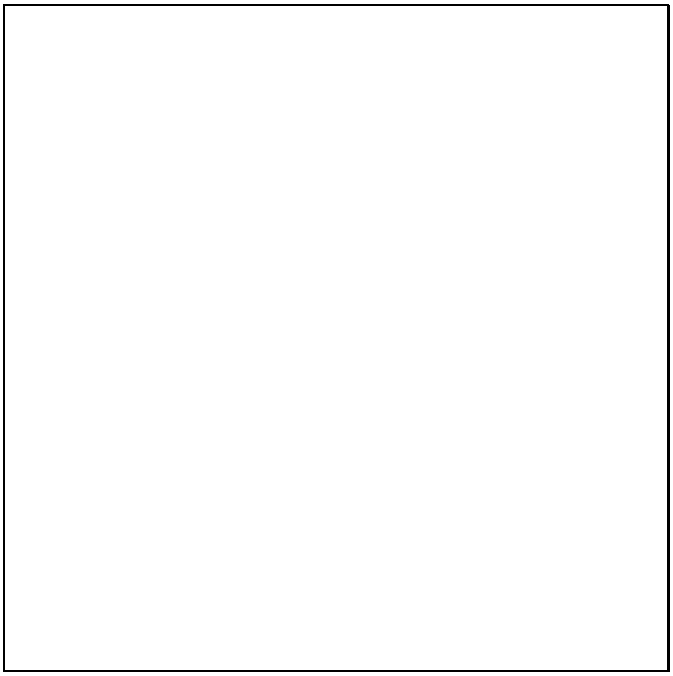

Fig. 5. The Hα luminosity function for outer HII regions of IZW18.

For IZW18 the small number of HII regions prevents a derivation of an accurate luminosity function, but nevertheless the data are sufficient to get a first approximation. In Fig. 5 the distribution of Hα luminosities binned in intervals of 1.0 10^{36}ergs s^{-1} is presented. The observed luminosity function of IZW18 shows a turnover with a maximum at $L = 3.0\ 10^{36}$ergs s^{-1} corresponding to the luminosity of the Orion nebula (Gebel 1968). This turnover is due to incompleteness towards fainter luminosities. At luminosities brighter than this turnoff the observed function is reasonably well fitted by a power law $N(L)=AL^{\alpha}dL$ with a slope α = -1.6±0.3. This is consistent with the mean value derived for dwarf irregular galaxies (Strobel et al. 1991) α = - 1.5±0.3. It may be compared with the steeper slope α = -1.7 found for larger irregulars by Kennicutt et al. (1989).

3.4. Hα velocity field

Figure 6 shows iso-velocity lines superimposed on the Hα gray scale image of IZW18. Figure 7 is a position-velocity cut across the optical major axis of the galaxy across the NW and SE compact components (PA = 143°). The shape of this position-velocity cut is in good agreement with slit 2 (PA = 156.1°) position-velocity diagram of M96.

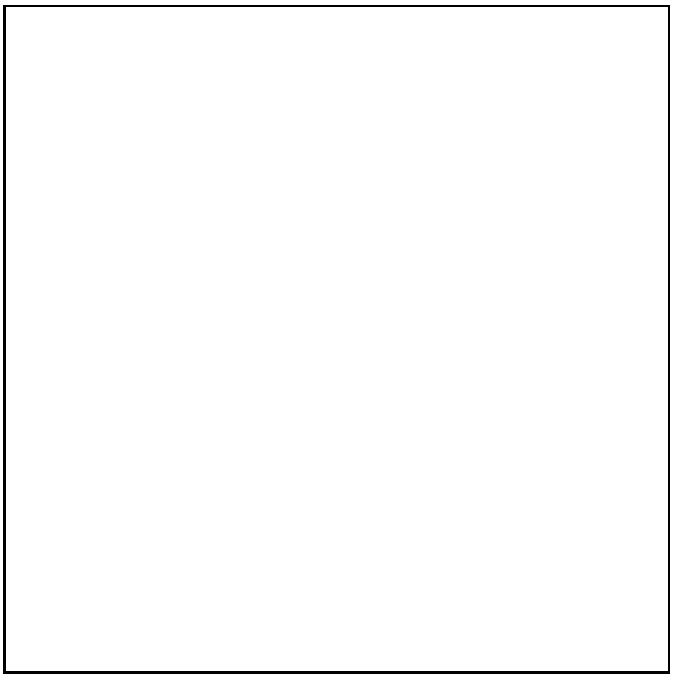

Fig. 6. Hα iso-velocity contour map of IZW18 superimposed on a gray scale image of the galaxy.

Figures 6 and 7 show a clear overall regular radial velocity gradient across the main body of IZW18. This finding obtained from the ionized gas confirms an earlier result by Viallefond et al. 1987 using HI aperture

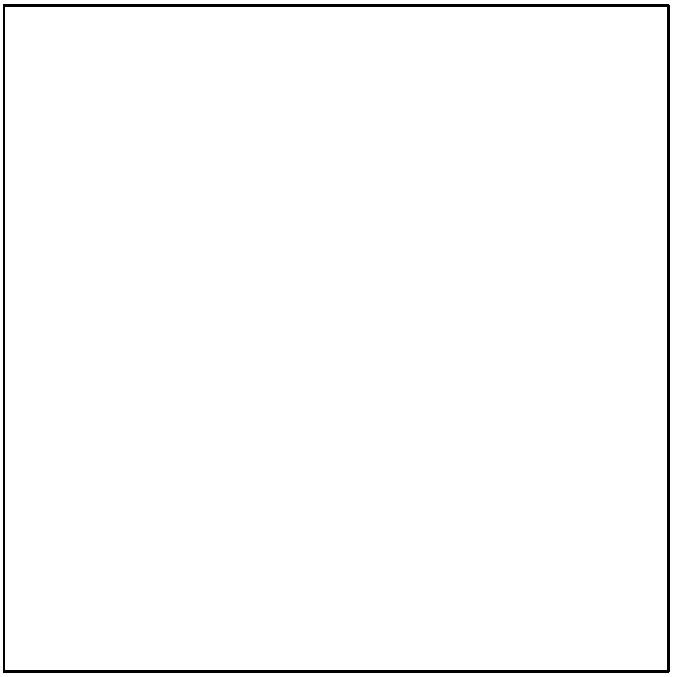

Fig. 7. Hα position-velocity cut across a line joining the NW and SE main compact HII components.

synthesis techniques. Fig. 7 further shows that the radial velocity gradient is globally consistent with a solid-body-like rotation of the ionized gas. The peaks of Hα emission in the NW and SE components are respectively centered at 739 km s^{-1} and 779 km s^{-1} and their average velocities are equal to 742±7 km s^{-1} and 783±5 km s^{-1}. These values are in agreement with those obtained using high-resolution spectroscopy (DKF89). They are also very similar to the Davidson & Kinman (1985) and HI velocity results (Lequeux & Viallefond 1980; Viallefond et al. 1987). The best symmetrical pattern of the velocity distribution is obtained along the major axis, when assuming a systemic recession velocity of 763 km s^{-1}. This value is in good agreement with the velocity of the number 5 HI cloud (765 km s^{-1}) in Lequeux & Viallefond (1980) and relates to a region which is very close to the red continuum component (a). Assuming that the radial velocity gradient, (which amounts to 73 km s^{-1} kpc^{-1} and is indicating a high mass concentration), is due to rotation (M96) we derive a Keplerian spherical mass of $1.910^8 M_\odot$ within a radius about 10 arcsec (480pc). Within this radius, we derive $M(HII) = 3.1\ 10^6 M_\odot$ for the mass of ionized gas. It corresponds to 1.6% of the total mass and about 40% of the neutral HI mass of the clump corresponding to the main body of IZW18 (Lequeux & Viallefond 1980; Viallefond et al. 1987). Within this limited radius, such a simple approximation is sufficient to derive a realistic estimate of the total mass. Any other more elaborate model will provide an estinate within a factor of 2 as compared to the Keplerian spherical mass.

Over the regular velocity field of IZW18 some complex structure is superimposed that locally modifies the isovelocity line and creates "bumps" at the position-velocity cut. These irregularities are particularly conspicuous in the NW region. Across a 70x70 pc^2 area located 150pc north from the peak intensity of the NW component we observe a local velocity excess of 15-17 km s^{-1}. The position of this excess coincides with the secondary peak in the spectrum of DFK89. It is also coincident with the location of the red continuum (b) component (Fig. 1, insert). This velocity structure has been previously discussed by M96 and by Skillman & Kennicutt (1993). The latter authors suggest a merging of two (or more) clouds rather than a pure solid body rotation. We dispute this interpretation using our previous statements on the regularity of the general velocity pattern and further note that the violent star formation that occurs in the NW compact component is likely to induce local peculiar gas motions. Other interesting velocity features relate to the ridge. In general the ridge follows the velocity distribution of the HI peak and IZW18 velocity field. Along the southern and part of the western length of the ridge, differences in radial velocities of the order of 10 - 15 km s^{-1} are found between its inner and outer regions. This difference is also evident across the slit 3 (PA=78.8°) position-velocity diagram of M96. No peculiar velocities were detected on the HII regions area of the ridge.

Coincident with Zwicky's "flare" a small Hα knot has a radial velocity of about 730 km s^{-1}. Therefore IZW18 and the Zwicky's "flare" belong to the same system. Those HII regions detected in the main body of IZW18 and its envelope (Sec.3.2) with sufficient S/N ratio exhibit radial velocities similar to that of the central velocity field.

3.5. Velocity dispersion distribution

Figure 8 and 9 display each individual Hα line profile superimposed to the Hα isophotal map of IZW18 in order to show the line profile structure of the outer envelope and the Hα line intensity distribution across the galaxy. Depending upon their location line profiles show different shapes. Typical unsmoothed Hα line profiles are shown in Fig. 10 together with the corresponding Gaussian fits. In all cases, the observed broad wings have instrumental origin and are most probably caused by adjacent orders.

Table 3 reports the results of the line profile analysis conducted on areas where the signal-to noise ratio is sufficient to achieve gaussian or multi-gaussian fitting of the observed Hα line. β(main) is the velocity dispersion of the main component of the line , corrected for thermal and instrumental broadening (Sec. 2); n(sec) is the number of secondary gaussian profiles fitting the observed Hα line; V(sec) is the peak velocity difference between the main and secondary gaussian components; I(sec)/I(main) is the intensity ratio of the secondary and main gaussian

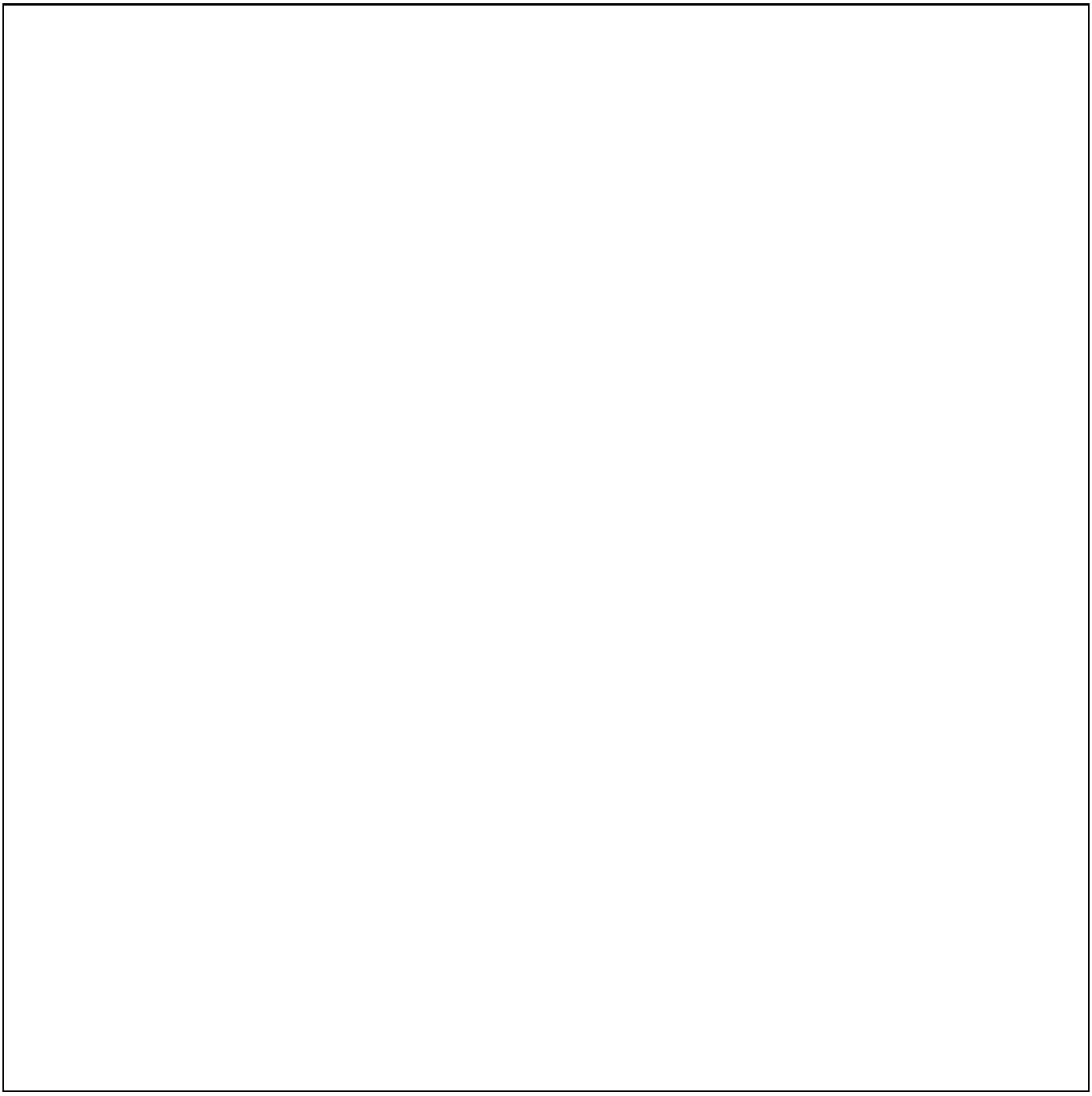

Fig. 8. Hα line profiles on IZW18. Each profile is normalized to the maximum intensity of each pixel. The horizontal axis of each box represents the free spectral range of 375 km s^{-1}. In the chart, south is in the top and east is in the right side.

components. The numbers in Table 3 are average values taking into account several pixels for each region.

The NW component Hα line profiles mainly appear symmetrical and well-represented by a one-component Gaussian fit (Fig. 10a). It is interesting to note that in Hα line a small red asymmetry appears towards the direction of the SE component. With the assumption that the component is a gravitationally bound system (Terlevich & Melnick 1981) the total mass of the system is estimated about 2 $10^7 M_\odot$ and the fraction of ionized gas in it as about 3%.

According to Skillman & Kennicutt (1993) a broad emission can be seen at the base of the Hα line profile for the NW component with a peak amplitude at about 0.2% of the main Hα line and a FWHM of about 80Å (about 3600 km s^{-1}). The small free spectral range (375 km s^{-1})

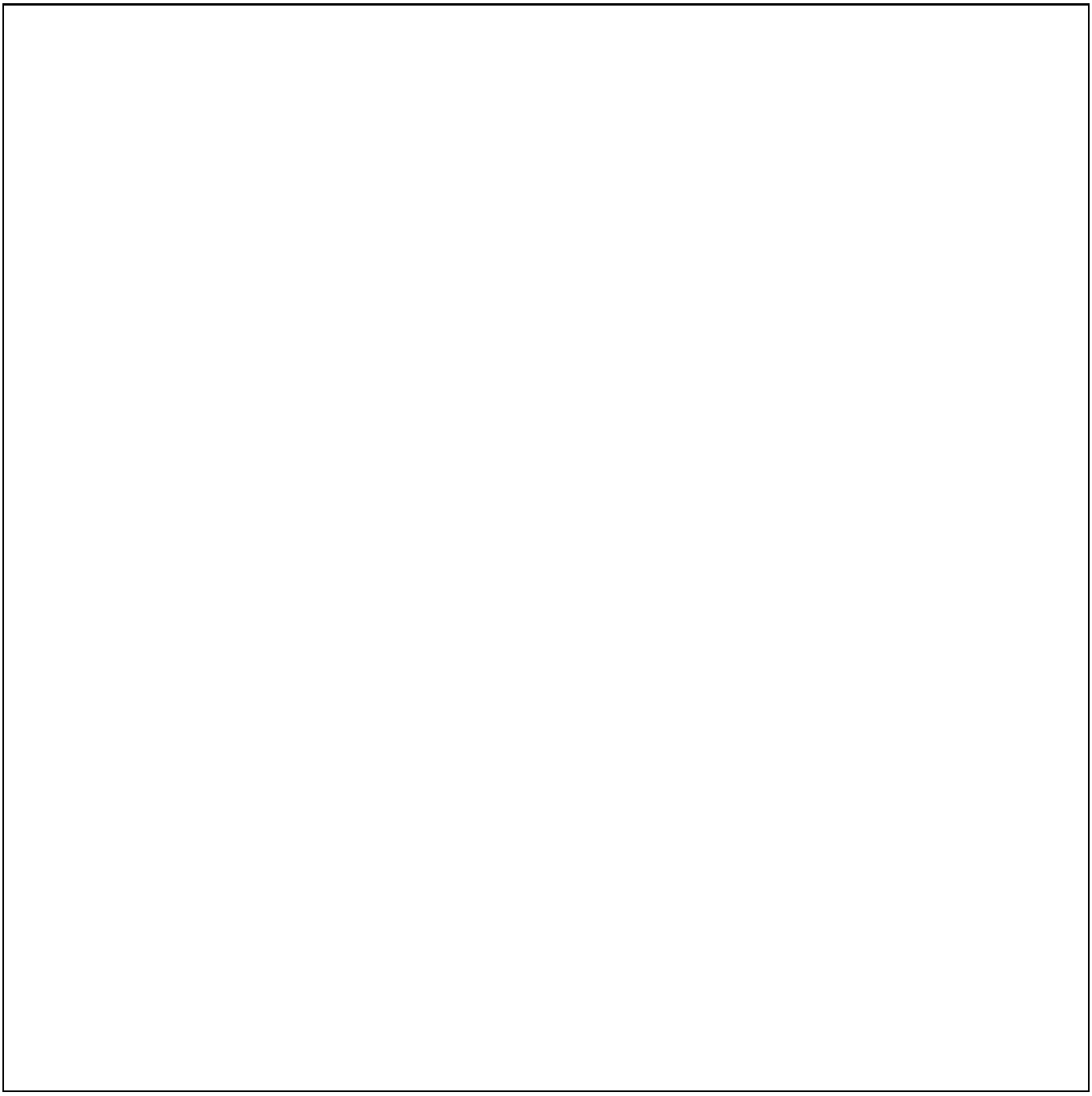

Fig. 9. The same as in Fig. 8 but each profile is normalized to the maximum intensity of the brightest pixel.

of the Fabry-Perot interferometer prevents to detect this broad component.

All Hα line profiles observed in pixels belonging to the SE component are asymmetric with blue side excesses (Fig. 10b). This blueshifted component contributes in average to 13% of the line flux and has a mean velocity of -50 km s^{-1} from the systemic velocity of the main component. Again, the small free spectral range of our observations (375 km s^{-1}) forbids the detection of faint large velocity components such as the ones found by M96 with velocities up to 230 km s^{-1} and A an intensity of about 3% of the main line flux.

Across the western part of the ridge (Fig. 10c) profiles with blue and red velocities excesses are typical. Usually redshifted components are more intense than blueshifted ones.

Across the southern part of the ridge profiles with strong blue side asymmetry are typical (Fig. 10d). Two

Table 3. Hα line profile analysis

		NW region	SE region	W ridge	S ridge
β $(main)$ $(km\ s^{-1})$		35.3 ± 1.6	26.5±0.4	16	16
n(sec)		0	1	2	2
V(sec)(km s^{-1})	1 :		-53.0±2.7	45.3±11.9	-40.7±3.2
	2 :			-39.0±7.0	-76.8±5.1
I(sec)/I(main)	1 :		0.15	0.30	0.40
	2 :			0.20	0.20

secondary components with 25% and 12% contributions of the line flux and -41 km s^{-1} and -77 km s^{-1} blueshifted from the systemic velocity of the main component were discovered. The bright knot well seen on the M96 Echelle spectrum at Hα along the slit position 1 (PA=7.7°) (see her Fig. 2) is caused by the southern part of the ridge. The two blueshifted components in the Hα profiles of the ridge are well separated in velocity (see Fig. 10d). This is well in agreement with the velocity range displayed in the M96 spectrum observed across the ridge position. On the so–called SW Doppler ellipse (M96), nearly 4″south from the ridge position, another fainter knot is observed that refers to our HII region number 23.

In the outer enveloppe of the main body of the galaxy, profiles are mainly asymmetric with red wings in the north-west and west of the SE component (M96), and with blue wings elsewere. In the NE Doppler ellipse of M96 (her Fig. 2), three other HII regions from our list have been identified as they appear as individual knots: number 9 and number 10 merged with number 12. All three HII regions have Hα line profiles with blueshifted components.

4. Discussion

4.1. The structure

The question still remains whether IZW18 is an old system in which some intense episodes of star formation already occured, or whether it forms stars for the very first time? Loose & Thuan (1986) reported observations of a faint outer component with an extended stellar continuum which they attributed to an underlying old population. Thuan (1983) detected infrared emission, while Hua et al. (1987), DFK89, DH90 from red continuum imagery, confirmed the presence of this component. The implication is that IZW18 may be an older and more complex system.

In the following, we make the assumption that Hα peaks relate to the current star–forming regions while red continuum features correspond to older sites of star formation. From the existence of the Hα loops and filaments HT95 also suggested the existence of intermitent star formation episodes in the central and northern parts of the galaxy. Their positions are in good agreement with our (a) and (b) red components.

The distribution of the clumps in the main body of IZW18 shows a chain–like structure. Out of seven identified current or more evolved star-forming knots six are distributed along the line SE,(a),NW,(b). This chain of star–forming knots is positioned along the direction of elongation of the main body of IZW18 and is consistent with HI outer clumps distribution (Lequeux & Viallefond 1980). Only knot (c) is displaced from this linear distribution.

In the chain both NW and SE currently active star–forming regions are located between more evolved star–forming sites. Is this geometry a random configuration? Does it examplify the sequential nature of star formation events in the galaxy (Gerola et al. 1980; Kunth et al. 1988) ? Clearly the chain although well ordered spatially does not define any prefered age sequence . Stochastic self-propagating star formation simulations of star formation sites in dwarf galaxies show that the properties of dwarf systems depend on the size ratio of the galaxy to the star formation cells. Small galaxies similar to IZW18 evolve mainly via a series of disconnected star forming bursts (e.g. Hunter & Gallagher 1985). Therefore, a stochastic origin of the observed "chain" is more plausible (see also HT95).

The ridge discovered by DH90 is thought to represent a radiation-bounded ionization front driven into the main HI cloud. Our red continuum data dispute this claim. Indeed the discovery of some stars in the ridge and surrounding regions (HT95) shows that the ridge contains a stellar population that can ionize the gas "in situ". Therefore the ridge is an isolated structure in the W-SW part of the double-peaked HI gas condensation and has no direct morphological link with the main body of IZW18.

Extended Hα emission have been detected up to distances of 1.5 kpc from the main body of IZW18. DH90, who noted the clumpy nature of this extended Hα emission, suggested that this emission could be powered by the central NW and SE star–forming complexes. M96 using imagery and high dispersion spectroscopy advocate that both north-east and south-west extensions of the outer envelope of the galaxy could be superbubbles powered by

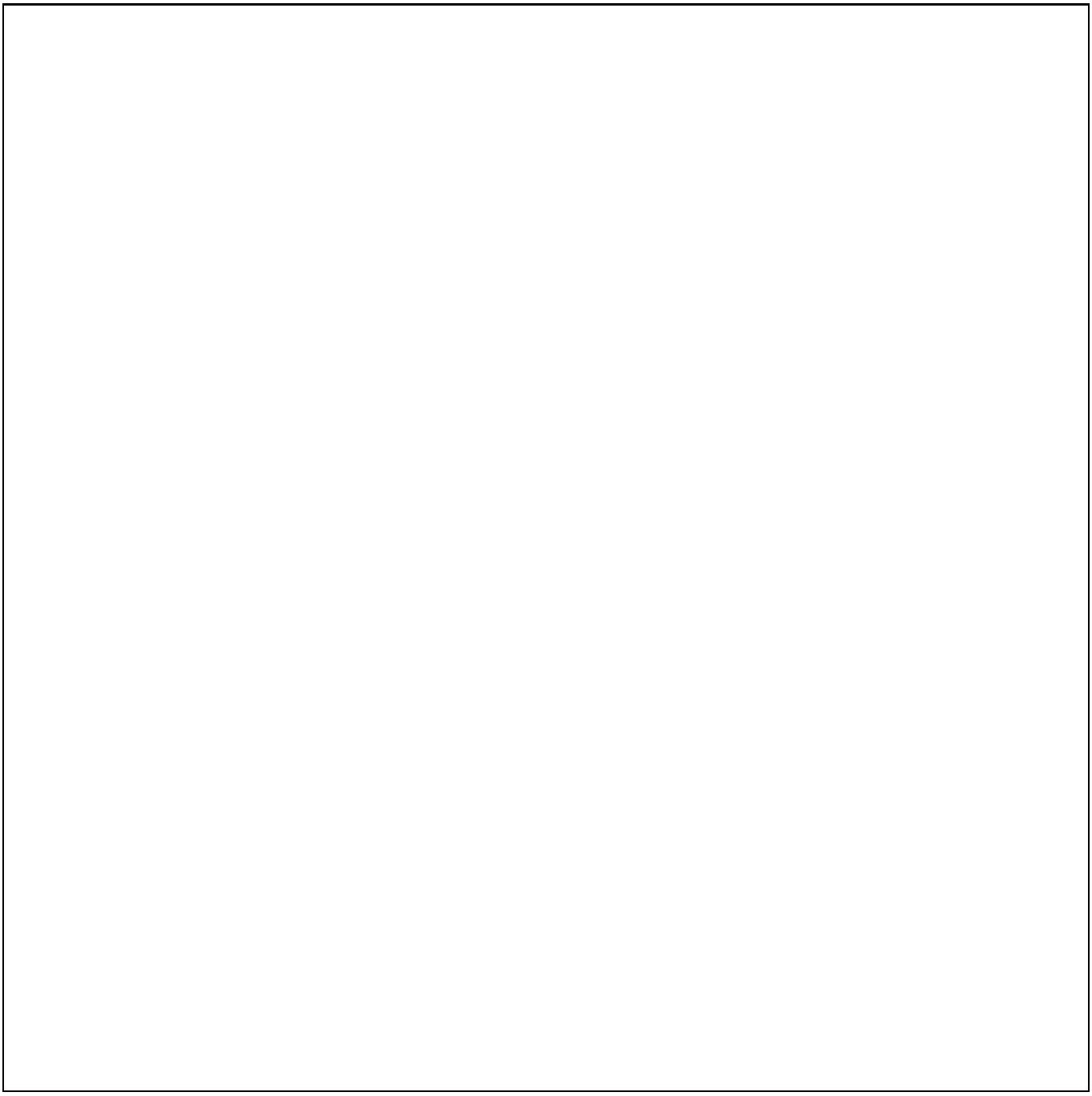

Fig. 10. Observed Hα profiles typical for: (a) NW and (b) SE components of IZW18; (c) for western part of the ridge and (d) southern part of the ridge. Broken lines are the fitted gaussian profiles. Ticks in velocity scale are separated by 17 km s^{-1}.

star–forming complexes. However the existence of clumpy red continuum emission of stellar origin coeval with the extended Hα emission, as well as the number of stars which were discovered in the same regions (HT95) consisting into compact and well individualized clumpy structure allow us to suggest that a stellar population is embedded into the ionized gas. Therefore part of the young stars from this population can ionize and produce the observed extended HII emission. As noted in Sec.3.3, the diameters distribution and a tentative Hα luminosity function of these HII regions are consistent with those of normal HII regions in dwarf irregular galaxies. The existence of the stellar and HII regions populations in NE and SW extensions of the outer envelope of IZW18 does not preclude the contribution of some superbubbles in the same regions.

4.2. The kinematics and dynamics

As previously suggested, star formation in the main body of IZW18 possibly occurs via a series of disconnected bursts as a result of density fluctuations in the interstellar medium near the HI clouds. What is the mechanism which triggers the subsequent star formation? The velocity field in an HII galaxy as well as in its surrounding HI cloud may indeed play an important role (Saito et al. 1992; Tomita et al. 1993).

The velocity gradient observed along the main star–forming regions, both in Hα (our results in Sec.3.4) and in HI (from the maps of Viallefond et al. 1987) is equal to about 70 km s^{-1}kpc^{-1}. The same gradient across the offseted HI peak distribution is only 50 km s^{-1}kpc^{-1} (Viallefond et al. 1987). It means that local HII as well as HI gas in the region of the optical galaxy rotates faster than the HI gas at its peak distribution.

The ordered component of the IZW18 velocity field shows a peak orbital velocity of about 50 km s^{-1}. Most irregular galaxies (giants as well as dwarfs), exhibit a solid body rotation with about the same peak orbital velocities of 50–70 km s^{-1} but with shallow velocity gradients of 5–20 km s^{-1}kpc^{-1} over the optically visible region (Hopp & Schulte-Ladbeck 1991; Shostak & Skillman 1989; Gallagher & Hunter 1984 and literature therein). The much higher velocity gradient in IZW18 arises from its much smaller linear scale, when compared to normal irregulars.

The disordered motions superimposed over the regular velocity field of IZW18 appear as sharp velocity jumps of 10 to 20 km s^{-1} occuring on scales of about 500 pc^2. These appear related to the main body of the galaxy, and suggest that the gas is not in equilibrum locally. Corresponding dynamical timescales could be of the order of few 10^6years (HT95). The gravitational effects of the (b) and (c) star–forming centers as well as explosive star–forming events may explain these local disturbances.

As regards to Hα line profiles, the discrepancy between a single Gaussian component with velocity dispersion of 23 km s^{-1} (e - folding width: 33 km s^{-1}) observed in a 40 arcsec and 21 arcsec apertures by Arsenault & Roy (1986) and the complex line structure seen at our resolution of 0.″725 per pixel is not a surprise. Gaussian-like smooth profiles obtained by Arsenault & Roy (1986) result from integration over many distinct components with different space velocities and emissivities. As examples we can recall high resolution observations of NGC604 by Rosa & Solf (1984), Hippelein & Fried (1984) in comparison with results for NGC604 presented by Arsenault & Roy (1986) and also the very interesting case of the giant HII region NGC2363 (Arsenault & Roy 1986; Roy et al. 1991; Roy et al. 1992).

The single Gaussian component observed in the NW compact HII region may suggest a self- gravitating system (Terlevich & Melnick 1981). In this case the expected velocity dispersion (Melnick et al. 1988) is about twice smaller than the observed one. This difference can be caused either by the gravity of the nearby located recent star–forming NW and (b) regions or/and the effects of turbulence. The chaotic morphology of the ionized gas in the component (HT95) as well as the existence of high velocity gas expanding shell (M96) may favor the latter effects. Application of gravitation - turbulence model in this case would be more reliable (Arsenault & Roy 1988).

In the SE compact HII region the velocity dispersion for the main Gaussian component (about 19 km s^{-1}) is also higher than expected from a self-gravitational model (Terlevich & Melnick 1981). Such an excess velocity dispersion can also be caused by the peculiar motions of several stellar clusters observed in the core of this component (HT95). The weaker second Gaussian component may be produced by another isolated HII region in the SE area, undistinguishable because of projection effects.

The ridge which has no direct morphological connection with the main body of IZW18 broadly follows the velocity field structure of the HI peak. The ridge is therefore co-rotating with the HI cloud and the main body of IZW18. The ridge as an isolated configuration is probably not in equilibrium. It expands in an opposite direction with respect to the HI gas showing local well determined infall and/or outfall of ionized gas. The geometry as well as the velocity field of the ridge are consistent with the "blister" interpretation . The complex structure of the Hα line profiles observed in the envelope showing a variable position-dependent asymmetry (blue and/or red wings) suggests that we are observing gas infall onto the main body of the galaxy, whatever the direction of observation and/or local ionization fronts. The blue asymmetric components are much more prominent on the eastern side, opposite to the major HI concentrations. It may be evidence that infall of gas clouds fuels the overall star formation in IZW18. But we do not exclude the possibility that the arc-like structure of the ridge can be affected by a tidal interaction between IZW18 and the Zwicky's "flare".

4.3. The nature of IZW18

From our data and data from the literature we examine the nature of IZW18 following the hypothesis first introduced by Searle & Sargent (1972) and further discussed by Kunth et al. (1986), Vigroux et al. (1986), Thuan (1987) that in general BCDGs may be considered as the low luminosity end of irregular galaxies. In Table 4 global characteristics and parameters related to star formation properties in IZW18 are compared with those of dwarf irregular galaxies.

The results of comparison may be summarized as follows.

1. IZW18 has an absolute luminosity consistent with that of an "average" dwarf irregular. The small linear size of IZW18 accounts for the high surface brightness of the optically visible component.

Table 4. IZW18 and Dwarf Irr properties

	IZW18	Ref	Dwarf Irr	Ref
M(B)	-13.9	Huchra (1977)	-14.5	Hunter & Gallagher (1985, 1986)
D (kpc)	0.9	Huchra (1977)	5.9	Hunter & Gallagher (1985, 1986)
$BSB(mag\ arcsec^{-2})$	21.3	Huchra (1977)	23.8	Hunter & Gallagher (1985, 1986)
$lgM(HI)_{\odot}$	7.8	Lequeux & Viallefond (1980)	8.3	Hunter & Gallagher (1985, 1986)
$V(max)(kms^{-1})$	50	This paper	60	Gallagher & Hunter (1984)
$dV/dr(km\ s^{-1}\ kpc^{-1})$	73	This Paper	10	Gallagher & Hunter (1984)
U - B	-0.76	Huchra (1977)	-0.44	Hunter & Gallagher (1985, 1986)
B - V	0.17	Huchra (1977)	0.36	Hunter & Gallagher (1985, 1986)
Largest HII reg.(pc)	170	This Paper	300	Hunter & Gallagher (1985)
D_0 (pc)	24	This Paper	25	Hodge (1983)
α	-1.6	This Paper	-1.5	Strobel et al. (1991)
$O/H(10^4)$	0.17	Dufour et al. (1988)	4.43	Hunter & Gallagher (1985, 1986)
$L(H\alpha)(L_{\odot})$	310^5	This Paper	310^4	Hunter & Gallagher (1985)
$SB(H\alpha)(L_{\odot}pc^{-2})$	9	This Paper	1.5	Hunter & Gallagher (1985)
$SFR(M_{\odot}yr^{-1}pc^{-2})$	$4\ 10^{-8}$	This Paper	10^{-10}	Hunter & Gallagher (1985)

2. HI masses of IZW18 and dwarf irregular galaxies of comparable blue luminosity and the clumpy structure of the HI distribution are similar. As for IZW18, star formation in dwarf irregulars is not simply related to the projected HI gas density (e.g. Allsopp 1978).

3. A rigid body rotation which is typical for the majority of dwarf irregular galaxies with similar peak orbital velocity is observed in IZW18. The size of IZW18 makes the velocity gradient across it at least 5 times higher than in irregular galaxies.

4. Except for two giant star–forming sites, IZW18 contains a population of faint HII regions. This population by its luminosity and diameter distribution does not differ from the HII region population in dwarf irregular galaxies.

5. In IZW18 besides an extended underlying older stellar population (Loose & Thuan 1986) we report the existence of recent star–forming clumps. These regions also are important components in dwarf irregular galaxies (Hunter & Gallagher 1986).

6. By their very blue color, high Hα luminosity and surface brightness and their high star formation rate per unit area, the current star–forming regions in IZW18 significantly differ from those in dwarf irregular galaxies.

We may conclude that IZW18 share many characteristics in common with dwarf irregulars except for its much higher level of star–forming activity per unit area. The large velocity gradient together with the locally complex velocity field (including peculiar gas motions responsible for the line profile asymetries) are most probably responsible for the star formation itself.

From the existence of recent star–forming regions seen in continuum, with no exact spatial coincidence with HII regions, we can possibly conclude that we are observing a major second burst of star formation in this object (e.g. Kunth et al. 1995). The first burst was completed about few tenth 10^6 years ago (e.g. HT95; M96) and the present one is extremely recent (Kunth & Sargent 1986). The age of the present burst may be estimated as no more than a few 10^6 years (Lequeux et al. 1981; Copetti et al. 1985).

5. Conclusions

The main results of Hα scanning Fabry-Perot investigations of IZW18 may be summarized as follows:
- In the main body of this galaxy, the *current* sites of active star formation, identified from the presence of prominent emission lines have ages of few 10^6 years and are spatially separated from red continuum clumps which are sites of recent star formation episodes with ages of about few tenth of 10^6 years. All star formation sites in the galaxy are separated from the compact HI cloud double-peaked core.

- The extended Hα emission seen in the envelope surrounding the central condensations exhibits a number of clumps which are thought to be a population of normal HII regions.

- The velocity field of the galaxy shows a regular pattern suggesting ordered solid-body rotation on which local disturbances are superimposed.

- The Hα line profiles have a complex structure, and except in the NW HII compact region, cannot be fitted by single gaussian components. The presence of blue and/or red wings in many points of the envelope suggests a generalized pattern of infalling (expelling) gas clouds onto (from) the central star–forming regions.

- The observed "ridge" is an isolated morphological structure in the system. It is a star–forming site separated with respect to the IZW18 main body by the HI cloud. The shape and orientation of this ridge can be due to tidal interation between IZW18 and the Zwicky's "flare".

- The SW and NE extensions of the outer envelope of the galaxy besides the ionized gas component connected to a supergiant shell-expanding superbubble (M96) also contain stellar as well as HII regions components.

- The near environment of the galaxy is likely to be polluted not only with gas processed by the central massive stars and driven out by superwinds but also by products of a more local stellar population.

When compared to the average characteristics of dwarf irregular galaxies, the basic properties of IZW18 (luminosity, HI mass, solid body rotation, normal HII region population, existence of current and recent star formation sites) are consistent with the hypothesis of an overall similarity between this blue compact dwarf galaxy and a typical dwarf irregular. The rigid-body rotational velocity gradient and the blue surface brightness, which depend on the linear scale are much larger in IZW18. The essential difference is that a high star formation activity (an order of two magnitudes in the SF rate per unit area which respect to that observed in a typical dwarf irregular) is concentrated in a small compact region.

Acknowledgments. We would like to thank Dr. Deidre Hunter for providing her HST-WFPC2 data for IZW18 and Dr. Miguel Mas-Hesse for his model calculations of stellar contribution at 6600 Å with respect to the nebular continuum. Part of this research was supported by PICS (Programme International de Cooperation Scientifique) #247 of CNRS between France and Armenia. The financial support of International Association for the Promotion of Cooperation with Scientists from the Independant States (INTAS) is gratefully acknowledged. A.R. Petrosian would like to thank the warm hospitality of Institut d'Astrophysique de Paris and Observatoire de Marseille during his stay. We also thank Jean Mouette for his help during the preparation of the figures.

References

Allsopp, N.J. 1978, MN, 184, 397
Arnault, P., Casoli, F., Combes, F., Kunth, D. 1988, A&A, 205, 41
Arsenault, R., Roy, J.-R. 1986, AJ, 92, 567
Arsenault, R., Roy, J.-R. 1988, A&A, 201, 199
Bertola, F., Casini, C., Bettoni, D., Galletta, G., Noreau, L., Kronberg, P.P. 1984, AJ, 89, 350
Boulesteix, J., Georgelin, Y.P., Marcelin, M., Monnet, G. 1983, SPIE Conf. Instr. Astron., 5, 445, 37
Copetti, M.V.F., Pastoriza, M.G., Dottori, H.A. 1985, A&A, 152, 427
Davidson, K., Kinman, T.D. 1985, ApJS, 58, 321
Davidson, K., Kinman, T.D., Friedman, S.D. 1989, AJ, 97, 1591 (DFK89)
Dopita, M.A. 1972, A&A, 17, 165
Dufour, R.J. 1986, PASP, 98, 1025
Dufour, R.J. Hester J.J., 1990, ApJ, 350, 149 (DH90)
Dufour, R.J. Garnett D.R., Shields G.A., 1988, ApJ, 332, 752
Gallagher, III J.S., Hunter, D.A. 1983, ApJ, 274, 141
Gallagher, III J.S., Hunter, D.A. 1984, ARA&A, 22, 37
Gebel, W.C. 1968, ApJ, 153, 743
Gerola, H., Seiden, P.E., Schulman, L.S. 1980, ApJ, 242, 517
Filippenko, A.V. 1982, PASP, 94, 715
Hippelein, H., Fried, J.W. 1984, A&A, 141, 49
Hodge, P.W. 1983, AJ, 88, 1323
Hodge, P.W., Lee, M.G. 1990, PASP, 102, 26
Hodge, P.W., Lee, M.G., Kennicutt, Jr. R.C. 1989,PASP, 101, 32
Hopp, U., Schulte-Ladbeck, R.E. 1991, A&A, 248, 1
Hua, C.T., Grundseth, B., Nguyen-Trong, T. 1987, Ap Let. Comm., 25, 187
Huchra, J.P. 1977, ApJS, 35, 171
Hunter, D. A. 1982, ApJ, 260, 81
Hunter, D.A., Gallagher, III J.S. 1985, ApJS, 58, 533
Hunter, D.A., Gallagher, III J.S. 1986, PASP, 98, 5
Hunter, D.A., Thronson, Jr. H.A. 1995, ApJ, 452, 238 (HT95)
Kennicutt, Jr. R.C., Edgar, B.K., Hodge, P.W. 1989, ApJ, 337, 761
Klein, U., Grave, R., Wielebinski, R. 1983, A&A, 117, 332
Kunth, D., Sevre, F. 1986, Star Forming Dwarf Galaxies, eds. D.Kunth, T.X.Thuan, J.T.T.Van, (Editions Frontieres) p.331
Kunth, D., Sargent, W.L.W. 1986, ApJ., 300, 496
Kunth, D., Maurogordato, S., Vigroux, L. 1988, A&A, 204, 10
Kunth, D., Lequeux, J., Sargent, W.L.W, Viallefond, F. 1994, A&A, 282, 709
Kunth, D., Matteucci, F., Marconi, G. 1995, A&A, 297, 634
Laval, A., Boulesteix, J., Georgelin, Y.P., Georgelin, Y.M., Marcelin, M. 1987, A&A., 175, 199
Lequeux, J., Viallefond, F. 1980, A&A, 91 ,269
Lequeux, J., Peimbert, M., Rayo, J.F., Serrano, A., Torres-Peimbert, S. 1979, A&A, 80, 155
Lequeux, J., Maucherat-Joubert, M., Deharveng, J.M., Kunth, D. 1981, A&A, 103, 305
Lequeux, J., Kunth, D., Mas-Hesse, J.M., Sargent, W.L.W. 1995, A&A, 301, 18
Loose, H.-H., Thuan, T.X. 1986, Star Forming Dwarf Galaxies, eds. D. Kunth, T.X.Thuan, J.T.T.Van, (Editions Frontieres), p. 73
Martin, C. 1996, ApJ, In Press (M96)
Mazzarella, J.M., Boroson, T.A. 1993, ApJS, 85, 27
Mazzarella, J.M., Bothun, G.D., Boroson, T.A. 1991, AJ, 101, 2034
Melnick, J., Terlevich, R., Moles, M. 1988, MN, 235, 297
Ostlin, G., Bergvall, N., Ronnback, J. 1996, in "The Interplay Between Massive Star Formation, The ISM and Galaxy Evolution", ed.Kunth D., Guiderdoni B.,Heydari-Malayeri T.X. Thuan , (Editions Frontieres), In Press
Osterbrock, D.E. 1989, Astrophysics of Gaseous Nebulae and Active Galactic Nuclei (University Science Books: Mill Valley,CA)
Pettini, M., Lipman, K. 1995, A&A, 297, L63
Petrosian, A.R., Saakian, K.A., Khachikian, E.E. 1978, Afz, 14, 69
Rosa, M., Solf, J. 1984, A&A, 130, 29
Roy, J.-R., Boulesteix, J., Joncas, G., Grundseth, B. 1991, ApJ, 367, 141
Roy, J.-R., Aube, M., McCall, M.L., Dufour, R.D. 1992, ApJ, 386, 498
Saito, M., Sasaki, M., Ohta, K., Yamada, T. 1992, PASJ, 44, 593

Sargent, W.L.W., Searle, L. 1970, ApJ, 162, L155
Searle, L., Sargent, W.L.W. 1972, ApJ, 173, 25
Shostak, G.S., Skillman, E.D. 1989, A&A, 214, 33
Skillman, E.D., Kennicutt, Jr.R.C. 1993, ApJ, 411, 655
Strobel, N.V., Hodge, P., Kennicutt, Jr.R.C. 1991, ApJ, 383, 148
Taylor, C.L., Skillman, E.D., Brinks, E. 1991, BAAS, 23, 920
Terlevich, R., Melnick, J. 1981, MN, 195, 839
Thuan, T.X. 1983, ApJ, 268, 667
Thuan, T.X. 1987, Starbursts and Galaxy Evolution, eds., T.Montmerle, T.X.Thuan, J.T.T.Van, (Edition Frontieres), p.129
Thuan, T.X., Williams, T.B., Malumuth, E. 1987, Star Bursts and Galaxy Evolution, eds.,T.Montmerle, T.X.Thuan, T.T.Van,(Editions Frontieres), p.151
Tomita, A., Ohta, K., Saito, M. 1993, PASJ, 45, 693
Tremaine, S., Gunn, J.E. 1979, Phys. Rev.Letters, 42, 407
Viallefond, F., Thuan, T.X. 1983, ApJ, 269, 444
Viallefond, F., Lequeux, J., Comte, G. 1987, Star Bursts and Galaxy Evolution,eds. T. Montmerle, T.X. Thuan, T.-T.Van, (Editions Frontieres), p.139
Vigroux, L., Stasinska, G., Comte, G. 1986, Star Forming Dwarf Galaxies, eds D. Kunth, T.X. Thuan, J.T.T. Van, Editions Frontieres, p. 425
Zwicky, F. 1966, ApJ, 143, 166

This article was processed by the author using Springer-Verlag LaTeX A&A style file *L-AA* version 3.